The Astrophysical Journal, 858:123 (6pp), 2018 May 10 https://doi.org/10.3847/1538-4357/aabaed

Interplanetary Shocks Inducing Magnetospheric Supersubstorms (SML < −2500 nT): Unusual Auroral Morphologies and Energy Flow

Rajkumar Hajra[1] and Bruce T. Tsurutani[2]
[1] Laboratoire de Physique et Chimie de l'Environnement et de l'Espace, CNRS, 3 Avenue de la Recherche Scientifique, F-45071 Orléans, France; rajkumarhajra@yahoo.co.in
[2] Jet Propulsion Laboratory, California Institute of Technology, 4800 Oak Grove Drive Pasadena, Pasadena, CA 91109, USA
Received 2018 February 18; revised 2018 March 27; accepted 2018 March 28; published 2018 May 15

Abstract

We present case studies of two interplanetary shock-induced supersubstorms (SSSs) with extremely high intensities (peak SML −4418 and −2668 nT) and long durations (∼1.7 and ∼3.1 hr). The events occurred on 2005 January 21 and 2010 April 5, respectively. It is shown that these SSSs have a different auroral evolution than a nominal Akasofu-type substorm. The auroras associated with the SSSs did not have the standard midnight onset and following expansion. Instead, at the time of the SML index peak, the midnight sector was generally devoid of intense auroras, while the most intense auroras were located in the premidnight and postmidnight magnetic local times. Precursor energy input through magnetic reconnection was insufficient to balance the large ionospheric energy dissipation during the SSSs. It is argued that besides the release of stored magnetotail energy during the SSSs, these were powered by additional direct driving through both dayside magnetic reconnection and solar wind ram energy.

Key words: magnetic reconnection – methods: data analysis – solar wind – Sun: coronal mass ejections (CMEs) – Sun: magnetic fields

1. Introduction

Substorms are typically midnight sector magnetospheric/ionospheric phenomena (Akasofu 1964) where the solar wind kinetic energy input into the Earth's magnetosphere/magnetotail occurs via dayside magnetic reconnection (Dungey 1961; Tsurutani & Meng 1972; Østgaard et al. 2005). According to the "standard substorm" scenario, auroras first brighten in a localized region of the equatorward-most midnight sector arc, then expand to the west, east, and poleward directions. The auroral electrojet current peaks in the area of the brightest aurora (e.g., Newell & Gjerloev 2011). The general magnetospheric scenario is that magnetic reconnection in the magnetotail leads to earthward convection of the plasma sheet into the outer regions of the magnetosphere where the auroral substorm onset occurs (e.g., Hones et al. 1973).

Interplanetary shocks (Gold 1955; Sagdeev 1966; Tsurutani et al. 2011) are known to trigger midnight sector substorms (e.g., Akasofu & Chao 1980; Zhou & Tsurutani 2001; Meurant et al. 2005). It has been shown that in general, precursor southward interplanetary magnetic fields (IMFs) are necessary ∼1.5 hr prior to shock impingement for a substorm to occur (Burch 1972; Zhou & Tsurutani 2001). Thus, Zhou & Tsurutani (2001) and Tsurutani et al. (2001) concluded that stored tail energy dissipation occurs rapidly. If a shock trigger does not occur within 1.5 hr of magnetotail energy loading, ever-present dissipation removes the stored energy. However, the previous authors did not study extreme substorms, the topic of this paper.

In this paper, we will examine two extremely intense and long-duration SML < −2500 nT events, defined as "supersubstorms" (SSSs) by Tsurutani et al. (2015). Hajra et al. (2016) identified 74 SSS events during the period from 1981 to 2012, which were shown to be externally triggered by small regions of very-high-density solar wind plasma parcels impinging upon the magnetosphere. However, the two SSSs of this study were unique events initiated simultaneously with interplanetary shock impingements onto the magnetosphere on 2005 January 21 and 2010 April 5. We will examine auroral images and the auroral electrojet currents to determine and characterize the morphology of these events. The main question to be answered by this paper is: do these SML/SSS events follow the morphology of lesser intensity, Akasofu (1964)-type substorms, or are they something different? The Akasofu definition of substorm evolution is considered the standard substorm model in this paper and will be referred to hereafter as such. For the SSS onset and end times we will be using the SML indices increases from background to peak intensity and then the decay to background once again. We will show how auroral images and magnetospheric evolution are associated with SML evolution.

2. Data Analyses and Results

2.1. SSS on 2005 January 21

Figure 1 shows the solar wind/interplanetary data in geocentric solar magnetospheric (GSM) coordinates and geomagnetic indices during 15:00–22:00 UT on 2005 January 21. The solar wind data collected from the OMNI database (http://omniweb.gsfc.nasa.gov/) have already been shifted in time to correspond to the arrival at the Earth's bow shock nose. Further temporal adjustments are not made. The SML index (Gjerloev 2009) based on ∼300 ground-based magnetometers of the SuperMAG network (http://supermag.jhuapl.edu/) can be used to determine the SSS onset, intensity, and duration. Three vertical lines in Figure 1 indicate the IMF Bz southward turning at ∼16:00 UT (red solid), the SSS onset at ∼17:11 UT (dashed), and the SSS SML peak at ∼17:38 UT (black solid). The SML index decreased sharply at ∼17:11 UT, indicating an intensification of the westward auroral electrojet (Figure 1(h)). After two consecutive decreases at ∼17:22 UT and ∼17:31 UT, the SML index attained a peak value of −4418 nT at

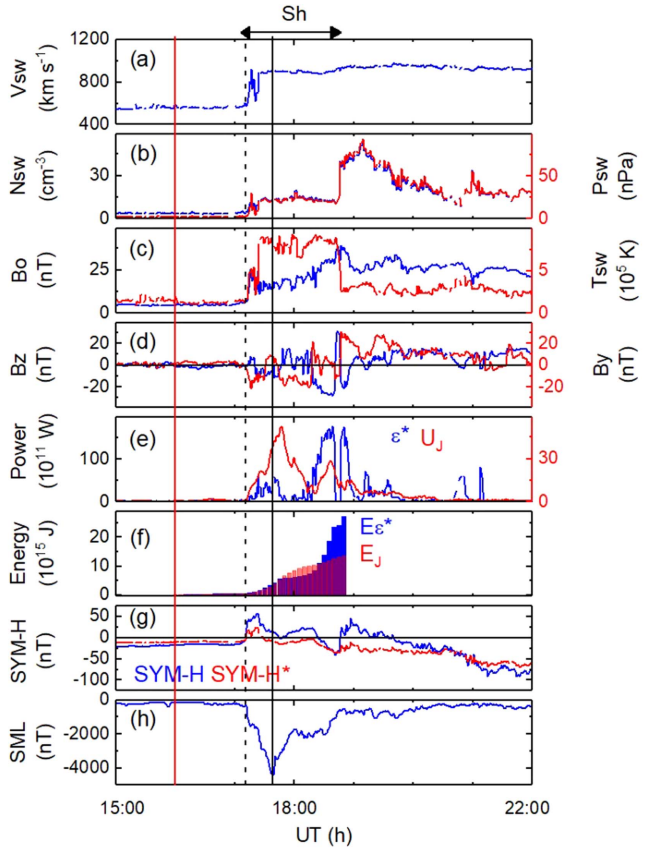

Figure 1. The SSS on 2005 January 21. From top to bottom, the panels show (a) the solar wind velocity Vsw, (b) density Nsw (blue, legend on the left) and the ram pressure Psw (red, legend on the right), (c) the interplanetary magnetic field magnitude IMF Bo (blue, legend on the left) and solar wind proton temperature Tsw (red, legend on the right), (d) IMF Bz (blue) and By (red), (e) ε^* (blue, legend on the left) and U_J (red, legend on the right), (f) $E\varepsilon^*$ (blue) and E_J (red), (g) SYM-H (blue) and SYM-H* (red), and (h) SML, respectively. The red dashed and black vertical lines indicate the IMF southward turning, and SSS SML onset and peak, respectively. The interval of the interplanetary magnetic sheath (Sh) is shown by the horizontal arrows on the top of the figure.

~17:38 UT. Following the peak SML value, SML increased sharply to −1710 nT at ~18:00 UT. Afterward, the SML index increased more slowly to the pre-substorm level at ~18:50 UT, indicating the end of the SSS. From the SSS onset to the SML peak, the substorm expansion phase continued for ~21 minutes, while the entire SSS event had a total duration of ~1 hr 40 minutes from the onset to end. The SSS had a more or less monotonic SML decrease and increase profile. During the SSS, the SYM-H index varied between ~+57 nT and ~−41 nT (Figure 1(g)). When corrected by removing the effects of the solar wind ram pressure and the quiet time ring current, SYM-H* varied between ~+29 nT and ~−39 nT (Burton et al. 1975; Gonzalez et al. 1989). No major magnetic storm (defined as Dst <−50 nT; Gonzalez et al. 1994) was in progress during this event.

The SSS onset at ~17:11 UT coincided with an interplanetary fast forward shock characterized by a jump in solar wind speed Vsw from ~560 to ~920 km s^{-1} (Figure 1(a)), in plasma density Nsw from ~4 to ~18 cm^{-3} (Figure 1(b), blue), in ram pressure Psw from ~3 nPa to ~30 nPa (Figure 1(b), red) and in IMF amplitude Bo from ~6 nT to ~25 nT (Figure 1(c), blue). Using the Abraham-Schrauner (1972) mixed-mode method and the Rankine–Hugoniot conservation equations (Smith 1985; Tsurutani & Lin 1985), the shock is found to have a magnetosonic Mach number of ~5.5 and a shock normal angle of ~81° relative to the upstream magnetic field. The shock and the high plasma density sunward of it caused a sudden impulse (SI$^+$) of ~+57 nT (see SYM-H in Figure 1(g)) and triggered the SSS event. The shock was related to an X7-class solar flare that erupted at a giant sunspot at ~07:00 UT on January 20. For detailed studies on the characteristics and impacts of this flare event, we refer the reader to Bombardieri et al. (2008), Saldanha et al. (2008), Pérez-Peraza et al. (2009), Wang et al. (2009), Firoz et al. (2012), Bieber et al. (2013), Tan (2013), and references therein.

The IMF Bz turned slightly southward at ~16:00 UT, marking the beginning of the solar wind energy input into the magnetosphere through magnetic reconnection (Figure 1(d), blue). During this phase, Bz varied from ~0 nT to a peak of ~−3.8 nT at ~16:23 UT. The SSS interval corresponds to an interplanetary magnetic sheath driver, characterized by multiple Bz changes with a peak value of ~−28 nT (Figure 1(d), blue), high plasma density Nsw ~20 cm^{-3} (Figure 1(b), blue), and high plasma temperature Tsw ~9 × 10^5 K (Figure 1(c), red). The SSS end coincided with an abrupt northward turning in IMF from ~−28 nT to ~+31 nT at ~18:41 UT. This is followed by the arrival of a solar filament at ~18:41 UT (see Kozyra et al. 2014). The SSS event was not associated with the filament. Apparently, the high density of the filament is what drove the shock to such a high Mach number and also the SI$^+$ to such an extremely high intensity.

Figures 1(e) and (f) show the "approximate" energetics of the SSS. Although an accurate measurement of the magnetospheric energy budget is not possible at this time, we use a modified Akasofu epsilon parameter ε^* (VswBo^2 sin$^4(\theta/2)R_{CF}^2$: Perreault & Akasofu 1978) to approximate the magnetospheric energy input rate. The Knipp et al. (2004) expression (a|PC| + bPC^2 + c|SYM-H| + dSYM-H^2) is used to estimate the ionospheric energy dissipation rate by Joule heating U_J. In the above expressions, θ is the clock angle of the IMF orientation, R_{CF} is the Chapman–Ferraro magnetopause distance (Chapman & Ferraro 1931; Shue & Chao 2013), PC is the polar cap index (Troshichev et al. 1988), and a, b, c, d are seasonal constants. The time-integrated magnetospheric input energy ($E\varepsilon^*$) and Joule dissipation energy (E_J) are estimated from the SSS start to finish. Prior to the SSS onset, the peak ε^* was low, ~3 × 10^{11} W. A total of ~0.6 × 10^{15} J energy was stored in the inner magnetosphere during this ~1.2 hr interval (through magnetic reconnection). During this interval, the peak U_J was ~2 × 10^{11} W and the total ionospheric energy dissipation was ~0.4 × 10^{15} J, ~67% of the input energy.

In the substorm expansion phase, ε^* attained a peak value of ~60 × 10^{11} W. Ionospheric Joule energy dissipated at almost the same rate (U_J ~ 53 × 10^{11} W). This may imply a direct energy driving process. We will discuss this later in more detail.

In the early SSS recovery phase, between ~17:45 UT and 18:25 UT, the estimated Joule dissipation energy (peak ~9.1 × 10^{15} J) is significantly larger than the estimated energy input (peak ~6.4 × 10^{15} J) through magnetic reconnection. This extra ionospheric dissipation may come from the magnetosphere/magnetotail system where energy has been stored. Large magnetospheric energy storage can be noted after ~18:25 UT. The ε^* had a peak of ~177 × 10^{11} W at ~18:39 UT. From the onset to the end of the SSS recovery, the total energy accumulated in the magnetosphere through IMF reconnection is estimated to be ~27 × 10^{15} J. The total

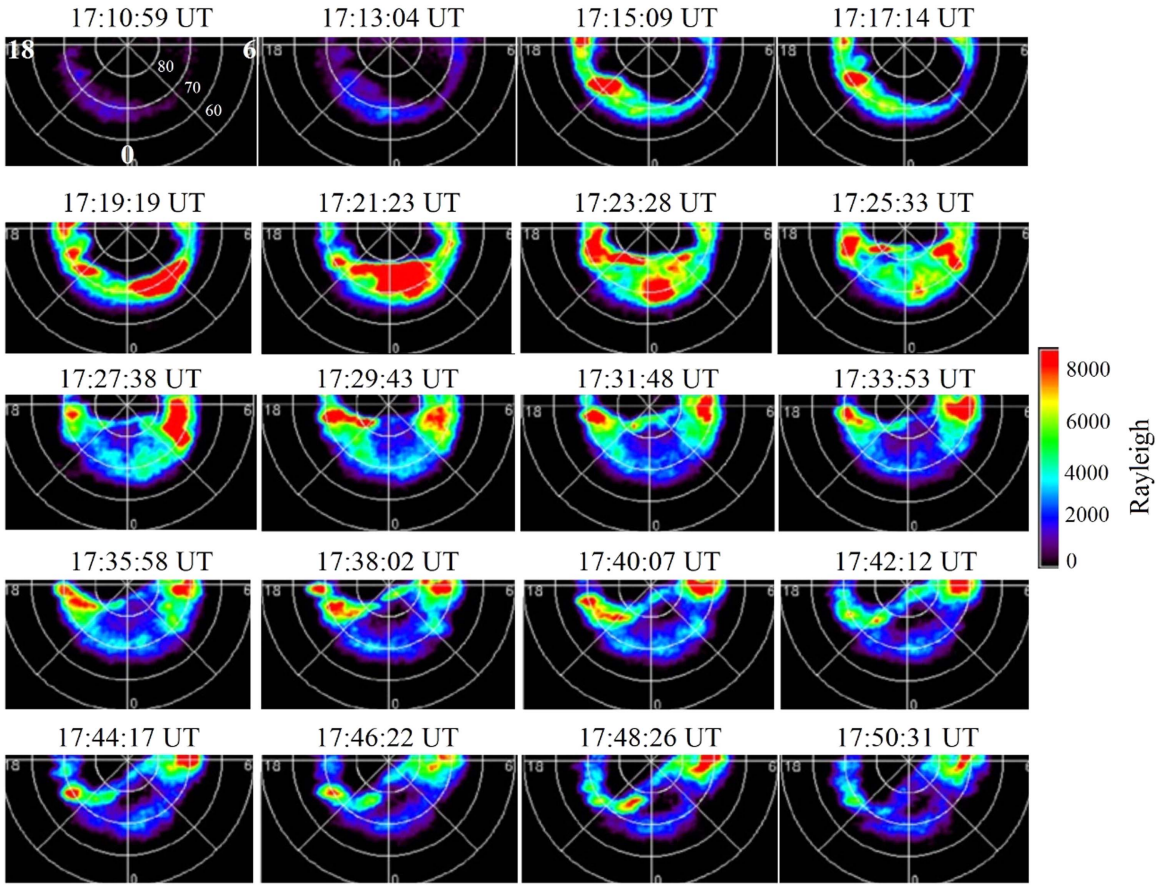

Figure 2. IMAGE-FUV all-sky images taken by WIC from ∼17:11 UT to ∼17:51 UT on 2005 January 21. The image cadence is ∼2 minutes.

ionospheric Joule dissipation over the same period is estimated to be $\sim 13 \times 10^{15}$ J or only ∼48% of the input energy. This excess energy input may be stored as a "primer" for subsequent geomagnetic activity.

Figure 2 shows the all-sky Wideband Imaging Camera (WIC) images in the far-ultraviolet (FUV: ∼1400–1800 Å) range taken by NASA's Imager for Magnetopause-to-Aurora Global Exploration (IMAGE; Frey et al. 2004) satellite from ∼17:11 UT to ∼17:51 UT on 2005 January 21. At ∼17:11 UT the pre-substorm auroral oval is found to be located at ∼70° magnetic latitude (MLAT). At ∼17:13 UT there is a small brightening at local midnight at ∼68° MLAT, which designates a small substorm onset that has often been called a "pseudobreakup" (Elvey 1957; Tsurutani et al. 1998; Aikio et al. 1999). About 2 minutes later at ∼17:15 UT, there is a strong premidnight (∼21:00 magnetic local time/MLT) brightening of the aurora at ∼68°–75° MLAT. At ∼17:19 UT, the most intense aurora is located at ∼68°–72° MLAT in the postmidnight/morning sector (∼00:00–04:00 MLT). The aurora moved from a dominant premidnight location to a postmidnight location in ∼2 minutes!

At ∼17:21 UT, the aurora intensified in the midnight sector (around 00:00 MLT) once more and expanded poleward to ∼80° MLAT. Strong auroral brightenings may be noted in the ∼00:00–03:00 MLT sector extending from ∼68° to ∼80° MLAT. At ∼17:23 UT, the midnight sector auroras start to dim and separate premidnight (∼21:00 MLT) auroral forms appeared at high latitudes (∼70°–80° MLAT).

By ∼17:26 UT the midnight aurora almost disappeared, while the premidnight aurora remained. At this time intense ∼03:00–04:00 MLT auroras became present at ∼68° to 80° MLAT. From ∼17:28 UT until ∼17:38 UT the premidnight and postmidnight high latitude (∼70°–80° MLAT) auroras are the most intense auroral features. There are very few intense auroras present in the midnight sector. It is shown in Figure 1 that all of the auroral forms discussed above occur prior to the peak SML value that occurred at ∼17:38 UT.

Starting at ∼17:30 UT and ∼17:32 UT are two interesting auroral features. This is the beginning of the interval where there was a lack of intense auroras in the midnight sector. The premidnight and postmidnight auroras are connected by slightly intensified auroras at both high and low latitudes. A similar phenomenon was reported previously by Tsurutani et al. (1998). The high latitude forms are as high as ∼85° MLAT (see the ∼17:32 UT image) and the low latitude forms are at ∼70° MLAT. These high and low latitude "connections" persist until ∼17:51 UT. This occurred during the most intense portion of the SML index, as shown in Figure 1.

It may be interesting to note that during the northward IMF turning around 17:38 UT, IMF By turned from positive to negative (Figure 1(d)). This interplanetary configuration is suggested to be conducive for generating transpolar auroral arcs connecting premidnight and postmidnight auroras, and leading to "theta aurora" (Frank et al. 1982; Cumnock et al. 2002; Fear et al. 2014, and references therein).

From ∼17:38 UT (the peak SML value) until ∼17:51 UT the locations of the premidnight and the postmidnight auroras

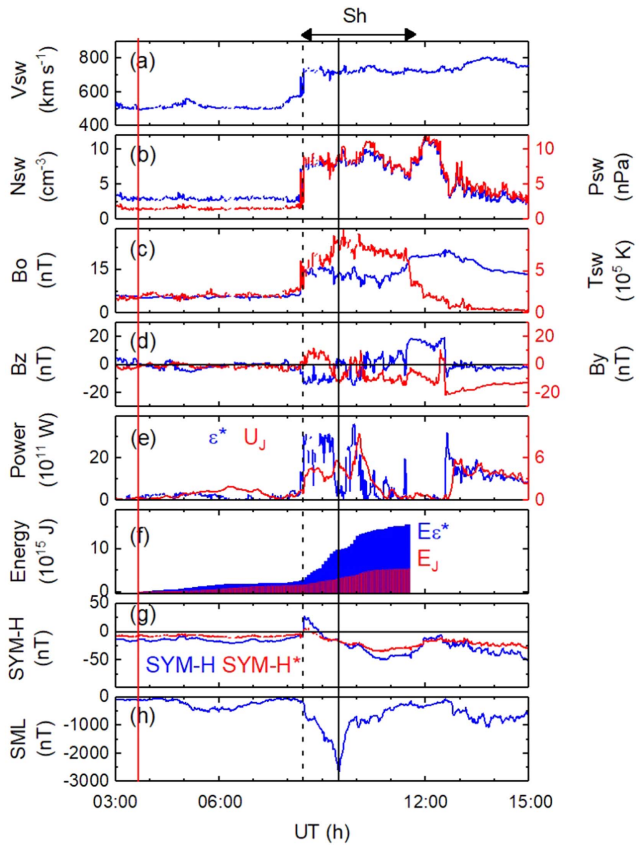

Figure 3. SSS on 2010 April 5. The panels are in the same format as in Figure 1.

evolved slowly. The premidnight aurora moved slightly closer to midnight and to lower MLATs. The postmidnight aurora moved to larger MLTs and even higher MLATs. It appears as if the auroral precipitation has rotated in MLT. At ∼17:40 UT, the premidnight aurora had moved from ∼19:00 MLT to ∼21:00 MLT at ∼70° MLAT. From ∼17:38 UT to 17:42 UT, the postmidnight aurora has migrated to ∼06:00 MLT and from ∼70° to 80° MLAT. The poleward connection between the premidnight and postmidnight forms moved to even higher MLAT values of ∼86°–87°, which is almost over the magnetic north pole!

It is possible that the interval shown in Figure 2 had multiple auroral brightenings, and extremely fast poleward and equatorward expansions (so that they were not detected in these snapshots with ∼2 minutes cadence). The overall event was initiated with a small brightening at ∼00:00 MLT in the auroral zone at ∼68° MLAT. This portion of the event had the standard substorm expansive phase scenario. After substorm initiation there was rapid evolution and possibly several other substorm onsets. However, at the maximum of the SML index (∼17:38 UT), there were no intense auroras in the midnight sector, only intense auroras in premidnight and postmidnight local times. This is significantly different from the standard substorm picture of auroral evolution during the expansion phase.

2.2. SSS on 2010 April 5

Figure 3 shows the solar wind/interplanetary data and geomagnetic indices during the SSS event occurring on 2010 April 5. Three vertical lines indicate when the IMF Bz turned slightly southward at ∼03:40 UT (red solid), the SSS onset at ∼08:26 UT (dashed), and the SSS SML peak at ∼09:29 UT (black solid), respectively. The substorm onset at ∼08:26 UT is indicated by a sharp decrease in the SML index (Figure 3(h)). After two further decreases at ∼08:47 UT and ∼09:17 UT, the SML index attained its peak value of −2668 nT at ∼09:29 UT. The SML recovered to its pre-substorm level at ∼11:34 UT. From onset to the peak, the SSS expansion phase had a duration of ∼1 hr 3 minutes, approximately three times the expansion phase duration of the 2005 SSS event. The 2010 SSS had a total duration of ∼3 hr 8 minutes from onset to end. Similar to the former SSS event, the SML profile was characterized by a smooth decrease and a smooth recovery, i.e., more-or-less monotonic variations with time. The SYM-H (SYM-H*) index varied between ∼+28 nT to ∼−49 nT (∼+6 nT to ∼−34 nT), indicating a non-storm time interval (Figure 3(g)).

The SSS onset coincided with a fast forward shock that is characterized by a jump in Vsw from ∼574 to ∼740 km s^{-1} (Figure 3(a)), in Nsw from ∼2 to ∼9 cm^{-3} (Figure 3(b), blue), in Psw from ∼2 nPa to ∼9 nPa (Figure 3(b), red), and in IMF Bo from ∼6 nT to ∼15 nT (Figure 3(c), blue). The shock had a magnetosonic Mach number of ∼2.9 and a shock normal angle of ∼54° relative to the upstream magnetic field. It caused a SI$^+$ in SYM-H of ∼+28 nT (Figure 3(g)).

The IMF Bz turned slightly southward at ∼03:40 UT, marking the beginning of energy input into the magnetosphere via magnetic reconnection (Figure 3(d), blue). During this phase, Bz varied from ∼0 nT to a peak of ∼−5.2 nT at ∼05:11 UT. The SSS interval corresponds to an interplanetary sheath driver. Multiple Bz polarity changes occurred within the sheath, with a peak negative value of ∼−14.2 nT. The sheath is characterized by high Nsw ∼10 cm^{-3} (Figure 3(b), blue) and high Tsw ∼9.9 × 10^5 K (Figure 3(c), red). An abrupt northward turning in IMF from ∼−8 nT to ∼+18 nT at ∼11:34 UT coincided with the SSS termination.

As in the case of the 2005 SSS event, the proxy precursor magnetospheric energy input rate ε^* was low (∼4 × 10^{11} W) owing to a weak IMF prior to the SSS onset (Figure 3(e), blue). A total of ∼3 × 10^{15} J energy was possibly stored during ∼4.8 hr prior to the SSS onset (Figure 3(f), blue). During this interval, the peak Joule heating rate U_J was ∼2 × 10^{11} W (Figure 3(e), red) and the total energy dissipation was ∼2 × 10^{15} J (Figure 3(f), red), ∼67% of the input energy.

During the SSS interval, ε^* attained a peak of ∼36 × 10^{11} W. Energy dissipated in the ionosphere at a significantly lower rate (∼9 × 10^{11} W) in the form of Joule heating. From the SSS onset to the end, in our scenario, the total energy accumulated in the magnetosphere is estimated as ∼16 × 10^{15} J (Figure 3(f), blue). The total ionospheric Joule dissipation over the same period is estimated to be ∼5 × 10^{15} J, or only ∼31% of the input energy (Figure 3(f), red).

Unfortunately, IMAGE-FUV images were only available for the 2005 event and not for the 2010 event. However, substorm evolution during the 2010 SSS can be studied by the Time History of Events and Macroscale Interactions during Substorms (THEMIS) project (http://themis.ssl.berkeley.edu/index.shtml; Angelopoulos 2008). Figure 4 shows raw keograms (in pixel row) from Athabasca (ATHA; 54°.71N, 246°.69E), White Horse (WHIT; 61°.01N, 224°.78E), Gakona (GAKO; 62°.41N, 214°.84E), Fort Yukon (FYKN; 66°.56N, 214°.79E), and Kiana (KIAN; 66°.97N, 199°.56E), obtained

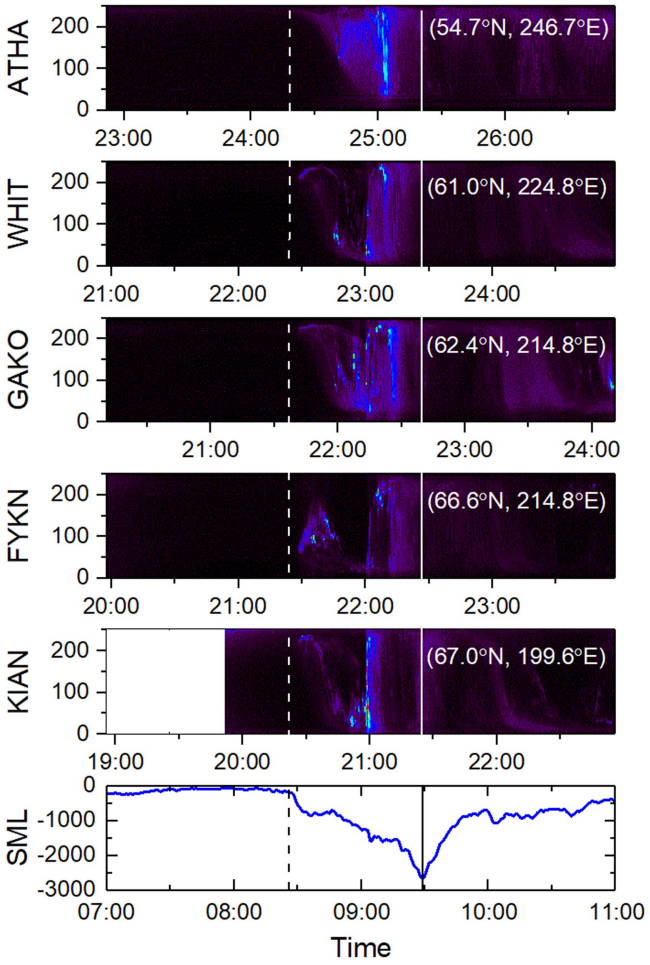

Figure 4. THEMIS keograms on 2010 April 5. The top five panels show the THEMIS ground-based raw keograms from ATHA, WHIT, GAKO, FYKN, and KIAN where the vertical axes are in pixel row. The bottom panel shows the SML index. The horizontal axis in the bottom panel gives the UT, while corresponding MLTs are shown for the keograms in the top panels. The vertical dashed and continuous lines indicate the SSS onset and SSS SML peak, as in Figure 3.

from ground-based high-resolution all-sky images of the THEMIS. With the interplanetary shock impingement (shown by vertical dashed line), auroral brightenings are recorded in keograms at the premidnight MLT sectors at KIAN (∼20:27 MLT), FYKN (∼21:29 MLT), GAKO (∼21:43 MLT), and WHITE (∼22:30 MLT). These correspond to the substorm onset (∼08:26 UT). No corresponding auroral brightenings were recorded in the midnight MLT sectors (23:00–25:00 MLT) at the substorm onset. In the substorm SML expansion phase, at ∼09:00 UT, another major auroral brightening was recorded at KIAN (∼20:59 MLT), FYKN (∼22:06 MLT), GAKO (22:20 MLT), WHIT (∼23:09 MLT), and ATHA (∼01:03 MLT). At the time of SML peak (∼09:29 UT, shown by vertical solid line), no midnight aurora was recorded. The strongest auroras were recorded in the premidnight magnetic local times. These are consistent with the IMAGE-FUV observations during the 2005 event.

3. Summary

This paper reports case studies of two long-duration, extremely intense substorms, or SSSs, induced by interplanetary shocks. The SML profiles for these events were more or less monotonic in shape, with slow, smooth decreases and smooth increases. The SSSs occurring on 2005 January 21 and 2010 April 5 had SML intensities of −4418 and −2668 nT. The expansion phase continued for ∼21 minutes and 1 hr 3 minutes, the SSSs had durations of ∼1 hr 40 minutes and ∼3 hr 8 minutes, respectively, from the onset to end. The multi-instrumental case studies may be summarized as follows:

1. The SSSs were induced by strong interplanetary shocks characterized by magnetosonic Mach numbers of 5.5 and 2.9, respectively (2005 and 2010 events). The shock normal angles were estimated to be 81° and 54°, respectively.
2. Simple magnetospheric energy proxy estimations show that the SSS onsets were preceded by low magnetospheric energy inputs of $\sim 0.6 \times 10^{15}$ J in ∼1.2 hr for the 2005 SSS event and $\sim 3 \times 10^{15}$ J in ∼4.8 hr for the 2010 event. There were only weak southward IMFs prior to the SSS onsets. These magnetospheric precursor energies were insufficient to supply the large ionospheric Joule dissipation energies ($\sim 13 \times 10^{15}$ J for the 2005 SSS, and $\sim 5 \times 10^{15}$ J for the 2010 SSS). Thus, precursor energy input through magnetic reconnection was not a viable mechanism for the SSS events. This result is different from that shown by Zhou & Tsurutani (2001) found for lesser intensity shock-induced substorms.
3. The auroral images during the initial portion of the 2005 SSS event showed some evidence of midnight sector substorm onsets or pseudobreakups, but the energy associated with them was minor compared with energy deposition in the premidnight and postmidnight sectors at the SSS peak intensity. For the 2010 SSS, the strongest auroral brightenings were recorded in the premidnight MLT sectors during the substorm expansion phase. This is considerably different from the standard substorm scenario where the majority of energy deposition is in the midnight sector.

4. Discussion and Conclusions

The SSS events studied in the present paper indicate a lack of standard auroral substorm evolutionary processes throughout their expansion phases. There were no simple brightenings of the equatorward-most midnight sector arc, auroral expansion, and recovery, as suggested by Akasofu (1964) for "typical substorms." It is possible that there were some standard substorm onsets within the SSS events, but because of the unusually fast evolution of auroral forms, it is not possible to verify whether or not this hypothesis is correct. However, when one examines the auroral images at the peak SML time, there are stable, intense auroral forms in the premidnight and postmidnight local time sectors, with a lack of intense auroras in the midnight sector. These features are very different from the standard typical substorms. It may be noted that the standard Akasofu substorm evolution was proposed as a simple guide for substorm studies based on a number of all-sky images without the benefit of detailed magnetogram and interplanetary data analysis. Thus, the present study indicates the importance of detailed and new multi-instrumental morphological studies to identify case-to-case variations of substorm evolution and energetics.

What exactly are these shock-triggered SSSs? Where does the energy come from to power the auroras? Our calculations based on magnetospheric energy proxies clearly show that magnetic reconnections either prior to shock arrivals or during the SSS

events themselves are insufficient to power the SSS events. Zhou & Tsurutani (2001) have argued that if there is no southward IMF prior to shock arrival, the shocks may not trigger even low-energy substorms. This is not the case for these two events. One possible explanation is that old, stored energy in the magnetosphere or tail lobes is being utilized in these extreme ram pressure events. Another possibility is direct energy input. We have shown that the energy input via magnetic reconnection matches that of Joule heating during the SSS events. A third source for direct magnetospheric energy input is solar wind ram energy. Clearly, the sudden ram compression drives field-aligned currents in the dayside outer magnetosphere (e.g., Zhou et al. 2003) powering direct Joule heating of the dayside ionosphere. Magnetospheric compression also directly compresses preexisting magnetospheric energetic particles, a source of dayside particle precipitation (Tsurutani et al. 2016). Could some of this direct energy input similarly be powering the nightside SSS auroras?

What are the causes of the observed auroras in the premidnight and postmidnight sectors? At this time we are not certain. However, because they are so long-lasting, a large percentage of the SSS energy must be deposited there. One possibility for the premidnight aurora is energetic proton drift into the duskside magnetosphere where the electromagnetic ion cyclotron waves are present (Cornwall 1965; Kennel & Petschek 1966). The postmidnight aurora might be a similar mechanism associated with a "dawn" chorus (Tsurutani & Smith 1977; Santolik et al. 2003; Bortnik et al. 2009). Further studies and modeling will be necessary to resolve these issues.

The work of R.H. is financially supported by Centre National d'Etudes Spatiales (CNES) through a postdoctoral research fellowship at LPC2E/CNRS. Portions of this research were performed at the Jet Propulsion Laboratory, California Institute of Technology under contract with NASA. The solar wind/interplanetary data at ~1 au were obtained from the OMNI database (http://omniweb.gsfc.nasa.gov/). The symmetric ring current index SYM-H was obtained from the World Data Center for Geomagnetism, Kyoto, Japan (http://wdc.kugi.kyoto-u.ac.jp/). The geomagnetic SML index was collected from the SuperMAG website (http://supermag.jhuapl.edu/). The WIC/FUV images taken by NASA's IMAGE satellite were obtained from http://sprg.ssl.berkeley.edu/image/. THEMIS keograms were obtained from http://themis.ssl.berkeley.edu/index.shtml.

ORCID iDs

Rajkumar Hajra https://orcid.org/0000-0003-0447-1531

References

Abraham-Schrauner, B. 1972, JGRA, 77, 736
Aikio, A. T., Sergeev, V. A., Shukhtina, M. A., et al. 1999, JGRA, 104, 12263
Akasofu, S. I. 1964, P&SS, 12, 273
Akasofu, S. I., & Chao, J. K. 1980, P&SS, 28, 381
Angelopoulos, V. 2008, SSRv, 141, 5
Bieber, J. W., Clem, J., Evenson, P., et al. 2013, ApJ, 771, 92
Bombardieri, D. J., Duldig, M. L., Humble, J. E., & Michael, K. J. 2008, ApJ, 682, 1315
Bortnik, J., Li, W., Thorne, R. M., et al. 2009, Sci, 324, 775
Burch, J. L. 1972, JGRA, 77, 5629
Burton, R. K., McPherron, R. L., & Russell, C. T. 1975, JGRA, 80, 4204
Chapman, S., & Ferraro, V. C. A. 1931, TeMAE, 36, 77
Cornwall, J. M. 1965, JGRA, 70, 61
Cumnock, J. A., Sharber, J. R., Heelis, R. A., et al. 2002, JGRA, 107, 1108
Dungey, J. W. 1961, PhRvL, 6, 47
Elvey, C. T. 1957, PNAS, 43, 63
Fear, R. C., Milan, S. E., Maggiolo, R., et al. 2014, Sci, 346, 1506
Firoz, K. A., Gan, W. Q., Moon, Y.-J., & Li, C. 2012, ApJ, 758, 119
Frank, L. A., Craven, J. D., Burch, J. L., & Winninghazn, J. D. 1982, GeoRL, 9, 1101
Frey, H. U., Mende, S. B., Angelopoulos, V., & Donovan, E. F. 2004, JGRA, 109, A10304
Gjerloev, J. W. 2009, EOSTr, 90, 230
Gold, T. 1955, in Gas Dynamics of Cosmic Clouds, ed. H. C. van de Hulst & J. M. Burgers (Amsterdam: NHPC), 103
Gonzalez, W. D., Joselyn, J. A., Kamide, Y., et al. 1994, JGRA, 99, 5771
Gonzalez, W. D., Tsurutani, B. T., Gonzalez, A. L. C., et al. 1989, JGRA, 94, 8835
Hajra, R., Tsurutani, B. T., Echer, E., Gonzalez, W. D., & Gjerloev, J. W. 2016, JGRA, 121, 7805
Hones, E. W., Jr., Asbridge, J. R., Bame, S. J., & Singer, S. 1973, JGRA, 78, 109
Kennel, C. F., & Petschek, H. E. 1966, JGRA, 71, 1
Knipp, D. J., Tobiska, W. K., & Emery, M. A. 2004, SoPh, 224, 495
Kozyra, J. U., Liemohn, M. W., Cattell, C., et al. 2014, JGRA, 119, 5401
Meurant, M., Gérard, J. C., Blockx, C., et al. 2005, JGRA, 110, A07228
Newell, P. T., & Gjerloev, J. W. 2011, JGRA, 116, A12211
Østgaard, N., Tsyganenko, N. A., Mende, S. B., et al. 2005, GeoRL, 32, L05111
Pérez-Peraza, J., Vashenyuk, E. V., Miroshnichenko, L. I., Balabin, Yu. V., & Gallegos-Cruz, A. 2009, ApJ, 695, 865
Perreault, P., & Akasofu, S. I. 1978, GeoJI, 54, 547
Sagdeev, R. Z. 1966, in Reviews of Plasma Physics, ed. M. A. Leontovich (New York: CB), 23
Saldanha, R., Krucker, S., & Lin, R. P. 2008, ApJ, 673, 1169
Santolik, O., Gurnett, D. A., Pickett, J. S., Parrot, M., & Cornilleau-Wehrlin, N. 2003, JGRA, 108, 1278
Shue, J. H., & Chao, J. K. 2013, JGRA, 118, 3017
Smith, E. J. 1985, in Collisionless Shocks in the Heliosphere: Reviews of Current Research, Vol. 35 ed. B. T. Tsurutani & R. G. Stone (Washington, DC: GMS), 69
Tan, B. 2013, ApJ, 773, 165
Troshichev, O. A., Andrezen, V. G., Vennerstrøm, S., & Friis-Christensen, E. 1988, P&SS, 36, 1095
Tsurutani, B. T., Arballo, J. K., Lakhina, G. S., et al. 1998, GeoRL, 25, 3047
Tsurutani, B. T., Hajra, R., Echer, E., & Gjerloev, J. W. 2015, AnGeo, 33, 519
Tsurutani, B. T., Hajra, R., Tanimori, T., et al. 2016, JGRA, 121, 10130
Tsurutani, B. T., Lakhina, G. S., Verkhoglyadova, O. P., et al. 2011, JASTP, 73, 5
Tsurutani, B. T., & Lin, R. P. 1985, JGRA, 90, 1
Tsurutani, B. T., & Meng, C. I. 1972, JGRA, 77, 2964
Tsurutani, B. T., & Smith, E. J. 1977, JGRA, 82, 5112
Tsurutani, B. T., Zhou, X. Y., Vasyliunas, V. M., et al. 2001, SGeo, 22, 101
Wang, J., Zhao, M, & Zhou, G. 2009, ApJ, 690, 862
Zhou, X. Y., Strangeway, R. J., Anderson, P. C., et al. 2003, JGRA, 108, 8019
Zhou, X. Y., & Tsurutani, B. T. 2001, JGRA, 106, 18957